JOURNAL OF MATERIALS SCIENCE 28 (1993) 649–653

Oxidation of monolithic TiB_2 and of Al_2O_3–TiB_2 composite

A. TAMPIERI, A. BELLOSI
CNR-IRTEC, Research Institute for Ceramics Technology, via Granarolo, 64 Faenza, Italy

In view of the susceptibility of TiB_2 to oxidation, the thermal stability of monolithic TiB_2 and Al_2O_3–TiB_2 composite was investigated. The temperature at which TiB_2 ceramic starts to oxidize is about 400 °C, oxidation kinetic being controlled by diffusion up to $T \approx 900$ °C and in the first stage of the oxidation at 1000 and 1100 °C (up to 800 and 500 min, respectively), and by a linear law at higher temperatures and longer periods. Weight gains of Al_2O_3–TiB_2 composite can be detected only at temperatures above ≈ 700 °C and the rate-governing step of the oxidation reaction is characterized by a one-dimensional diffusion mechanism at $T = 700$ and 800 °C and by two-dimensional diffusion at higher temperatures. The composition and morphology of the oxidized surfaces were analysed.

1. Introduction

Titanium diboride has been studied extensively for its potential applications, and has received great attention because of its high melting point, hardness, electrical conductivity and wettability by molten aluminium [1–3]. The addition of TiB_2 to an Al_2O_3 matrix greatly increases hardness, strength and fracture toughness; in addition, the Al_2O_3–TiB_2 composite can be used as electrodes, wear parts, cutting tools, high-temperature heaters [4, 5] and heat exchangers. Therefore, it is important to evaluate the thermal stability of monolithic TiB_2 and of Al_2O_3–TiB_2 composites because in use they can be exposed to oxidizing environments.

2. Experimental procedure

Starting with a commercial TiB_2 powder (Starck, Grade F), dense TiB_2 ceramics were obtained through hot pressing at 1850 °C for 60 min and at 30 MPa [3]. Al_2O_3–TiB_2 composites were produced by adding 30 vol % TiB_2 to Al_2O_3 (Alcoa A16 S.G.) and by hot pressing the mixture at 1600 °C, 30 MPa for 30 min [6].

The typical microstructures of TiB_2 (Fig. 1a, b) and of Al_2O_3–TiB_2 (Fig. 2a, b) show the grain size and morphology of the phases constituting the materials. Microstructure and mechanical properties are reported in Table I, detailed results have been reported elsewhere [3, 6].

As crystalline phases, in the monolithic sample, only TiB_2 was detected; in the composite, in addition to Al_2O_3 and TiB_2, the presence of some aluminium borates indicates that a limited reaction between the matrix and the dispersoids occurred during sintering.

Short-term oxidation tests (20–30 h) were carried out in a static air atmosphere on samples diamond sawn from the hot-pressed billets, then polished and cleaned. The weight gains were continuously recorded by a thermogravimetry–differential thermal analysis (TG–DTA) apparatus (Stanton Redcroft, UK), oxidation temperatures ranged from 400–1100 °C, and the heating rate was 30 °C min^{-1}.

The surface of the oxidized samples was analysed by X-ray diffraction (XRD, Rigaku Corporation), scanning electron microscopy (SEM, Autoscan, ETEC, USA), including back-scattered electron imaging, and energy – dispersive spectroscopy (Philips, EDAX PV 9100).

3. Results and discussion

Under isothermal conditions, weight gains ($\Delta W/S$, where ΔW is the weight gain and S is the surface of the sample) were detected starting at about 400 °C for TiB_2 (Fig. 3a) and at about 700 °C for Al_2O_3–TiB_2 (Fig. 3b).

3.1. Structure and morphology of the oxidized surfaces

The evolution of the crystalline phases content for the oxidized samples as derived from semiquantitative XRD are shown in Fig. 4a and b, for TiB_2 and Al_2O_3–TiB_2, respectively. The presence of crystalline TiO_2 was detected at temperatures higher than ≈ 700 °C in Al_2O_3–TiB_2 and ≈ 400 °C in TiB_2. The oxide scale in monolithic TiB_2 samples is also formed by crystalline B_2O_3 at $T = 700$–800 °C. However at $T > 800$ °C only highly textured TiO_2 crystals are detectable. In fact, epitaxial growth of rutile crystals occurs in the [2 1 1] and [1 0 1] directions, as previously observed [7, 8].

On the oxidized surface of Al_2O_3–TiB_2, the amount of rutile rapidly increases at $T > 700$ °C and two aluminium borate phases, $Al_4B_2O_9$ at 700 °C $\leqslant T \leqslant$

0022–2461

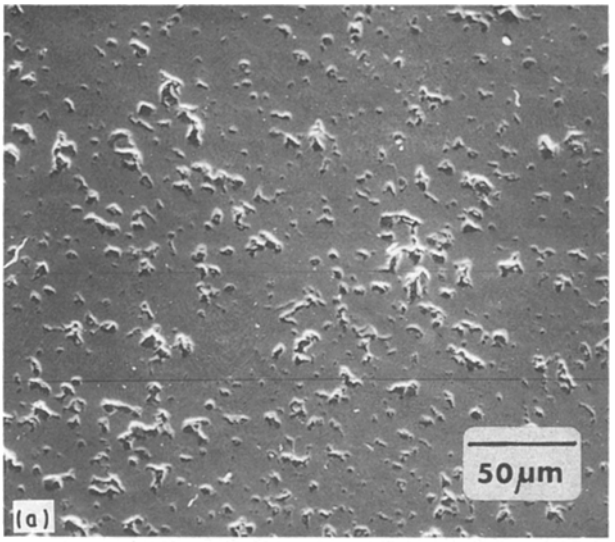

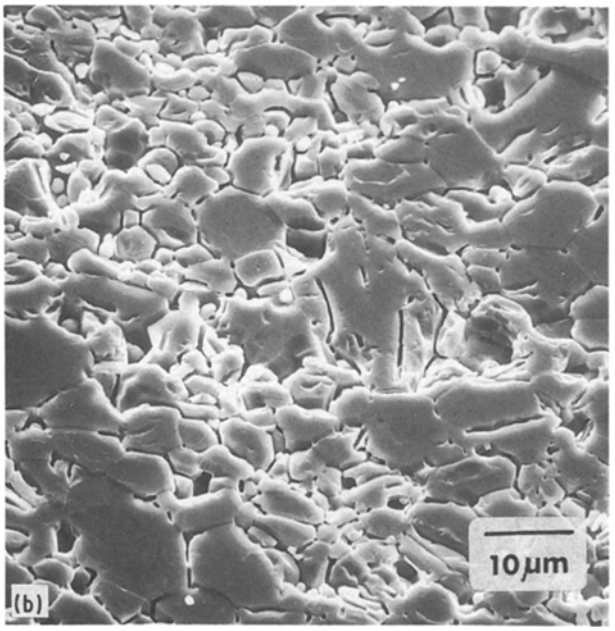

Figure 1 Microstructure of TiB_2 material: (a) polished surface; (b) polished and etched surface.

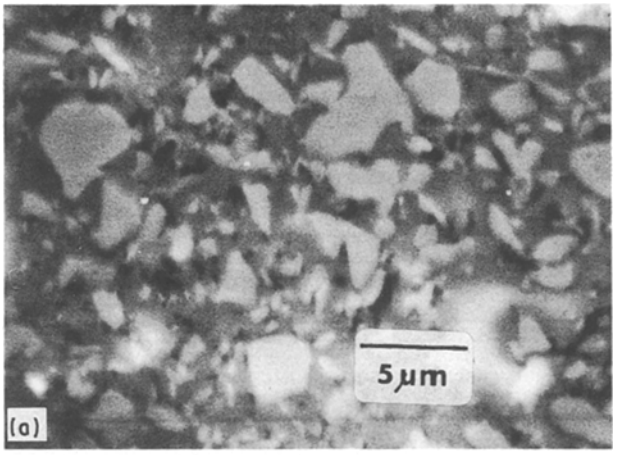

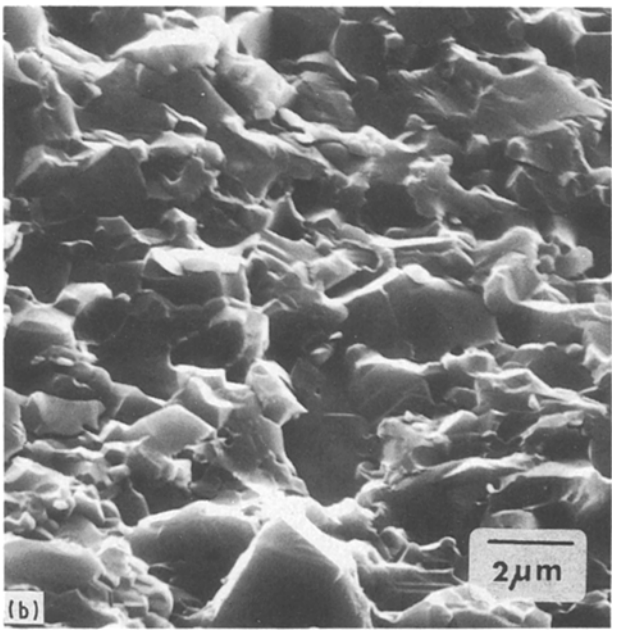

Figure 2 Microstructure of Al_2O_3–TiB_2 composite: (a) polished surface; (b) fracture surface.

900 °C and $Al_{18}B_4O_{33}$ at $T > 900$ °C, were observed. Both rutile and aluminium borate appear highly oriented on the surface of samples oxidized at $T \geqslant 1000$ °C.

Fig. 5a–c show the evolution of the morphology of the oxide scale in the monolithic TiB_2 after oxidation runs of 30 h. At $T \approx 400$ °C, an amorphous layer with some cracks and bubbles covers the surface. At $T \geqslant 1000$ °C, TiO_2 crystals form a thick oxide scale.

Fig. 6a–c show the microstructures of the oxidized surfaces of Al_2O_3–TiB_2 composites. Even at very low temperatures, $T \approx 400$ °C (Fig. 6a), in spite of the lack of weight gain, the oxidation produces pits and small cracks; at $T \geqslant 700$ °C (Fig. 6b) the surface is rough and completely covered by aggregates of needle-like or rod-shaped crystals. The dimensions of these crystals increase on increasing the oxidation temperature, at $T \approx 1000$ °C (Fig. 6c); the aluminium borate phase shows an aggregate morphology composed of highly oriented vertical rod-shaped crystals; rutile forms a layer of rounded crystals, which also show a preferred orientation. The back-scattered electron image of the surface oxidated at 700 °C (Fig. 7) shows bright areas which probably correspond to crystalline rutile and dark areas to aluminium borates.

TABLE I Properties of monolithic TiB_2 and Al_2O_3–30 vol % TiB_2 composite

Sample	ρ (Ω cm)	$\bar{\alpha}$ (10^{-6} °C^{-1})	E (GPa)	$H_{v_{0.5}}$ (GPa)	K_{IC} (MPa m$^{1/2}$)	σ (MPa)
TiB_2	1.4×10^{-5}	7.45	554	24.4 ± 1.0	5.4 ± 0.8	473 ± 19
Al_2O_3–TiB_2	1.4×10^{-3}	7.82	424	19.2 ± 0.8	5.7 ± 0.6	711 ± 9

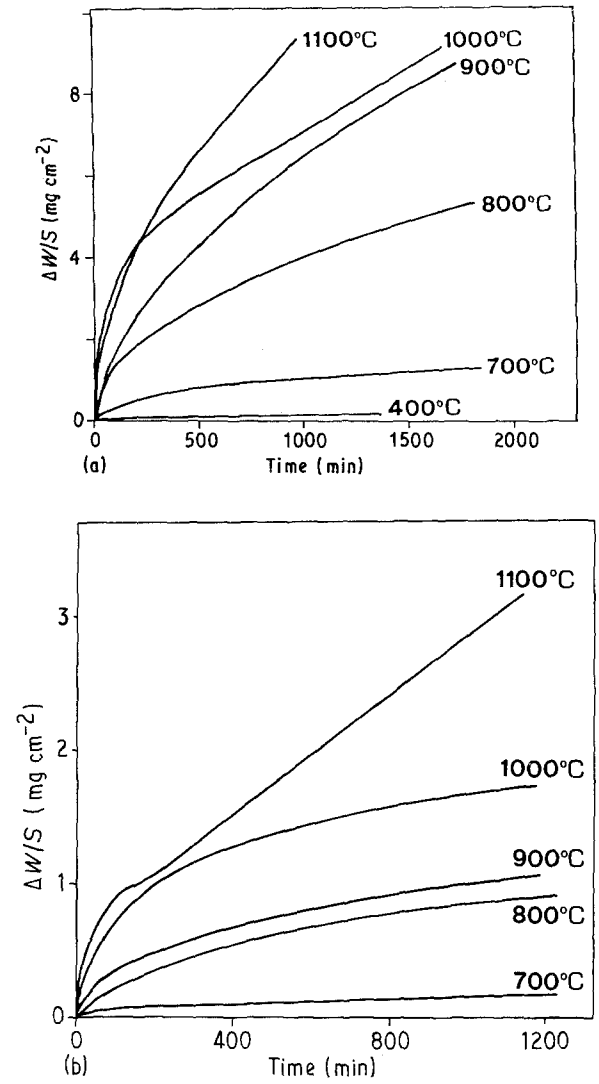

Figure 3 Isothermal weight gain at various temperatures for (a) TiB_2, and (b) Al_2O_3–TiB_2.

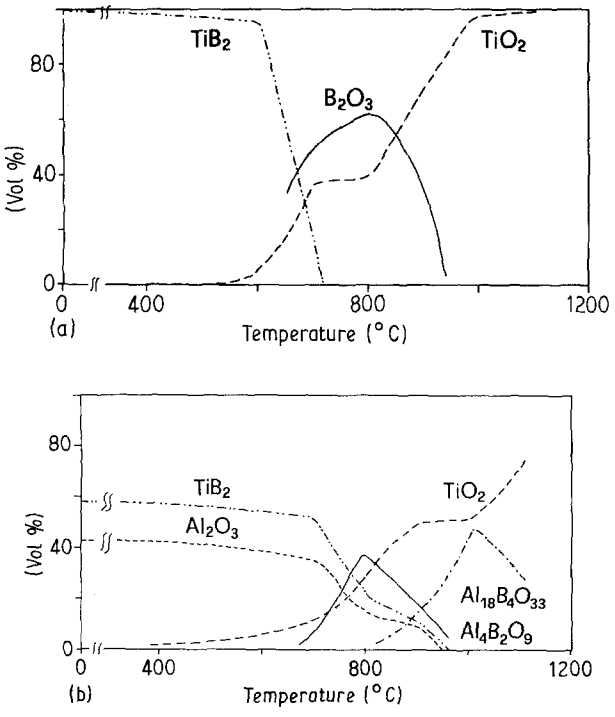

Figure 4 Semiquantitative X-ray analysis of the oxidized surfaces showing the crystal phase content: (a) TiB_2; (b) Al_2O_3–TiB_2.

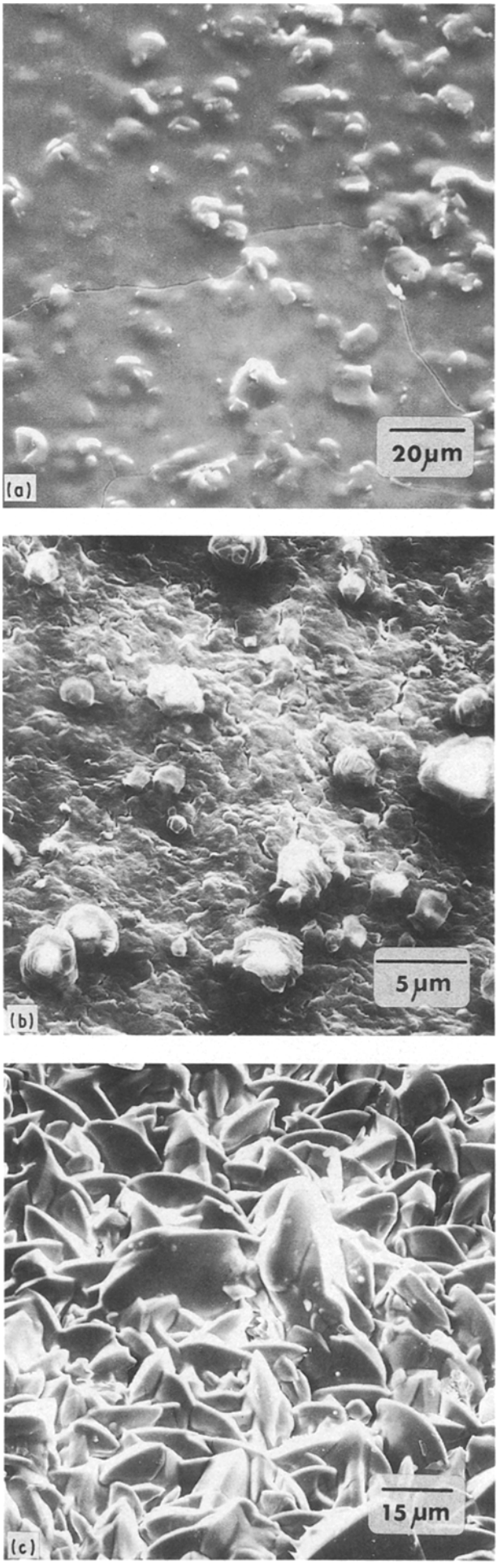

Figure 5 Evolution of the microstructure on the oxidized surfaces of TiB_2 after 30 h at (a) 400 °C, (b) 800 °C and (c) 1000 °C.

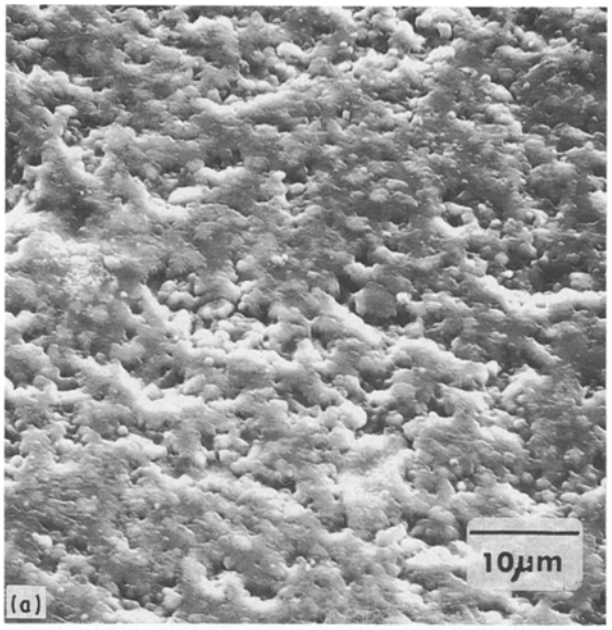

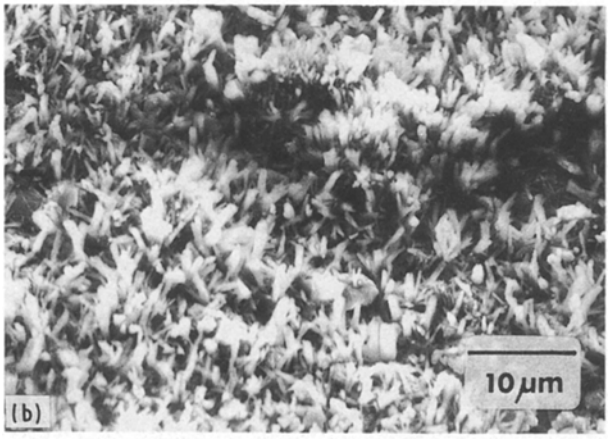

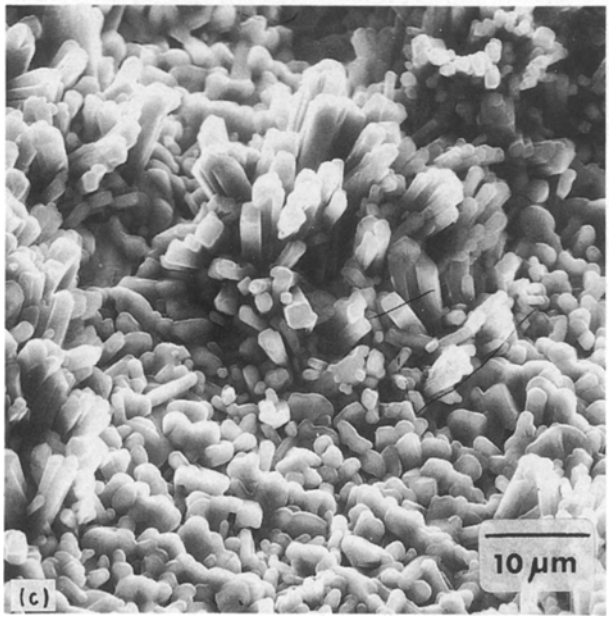

Figure 6 Morphology of the oxidized surface of Al_2O_3–TiB_2 at (a) 400 °C, (b) 700 °C and (c) 1000 °C.

3.2. Oxidation kinetics and mechanism

It is well known that TiB_2 oxidizes according to the chemical reaction

$$TiB_2 + 5/2\ O_2 \rightarrow TiO_2 + B_2O_3 \quad (1)$$

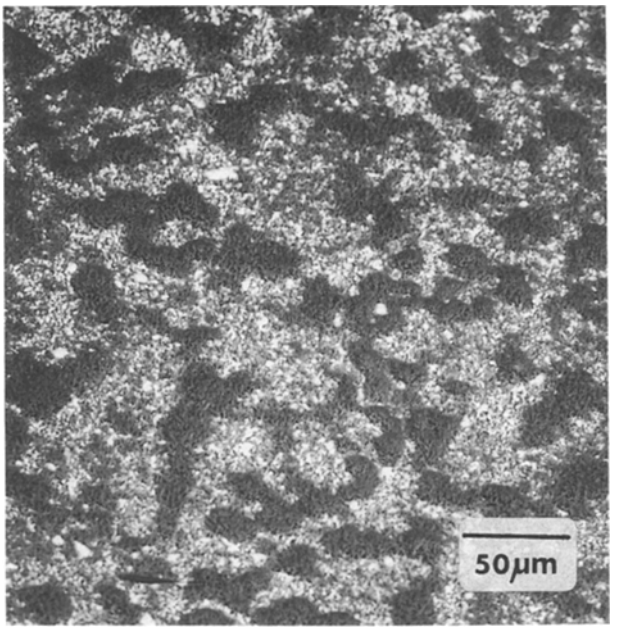

Figure 7 Back-scattered electron image of the 700 °C oxidated surface of Al_2O_3–TiB_2.

Crystalline B_2O_3 has been observed in the monolithic TiB_2 after oxidation at $T = 700$ and 800 °C. In Al_2O_3–TiB_2, following Reaction 1, further reactions occur

$$B_2O_3 + 2Al_2O_3 \rightarrow Al_4B_2O_9 \quad \text{at } T < \approx 900\,^{\circ}C \quad (2)$$

$$2B_2O_3 + 9Al_2O_3 \rightarrow Al_{18}B_4O_{33} \quad \text{at } T > \approx 900\,^{\circ}C \quad (3)$$

3.2.1. Monolithic TiB_2

The set of curves in Fig. 3a may be fitted using two kinetic models.

1. Diffusion-controlled kinetics $(\Delta W/S)^2 \approx Kt$, where K is the oxidation rate constant, valid up to $\approx$ 900 °C for the entire isothermal run, at 1000 °C up to about 800 min, and at 1100 °C up to $\approx$ 500 min.

2. Linear behaviour $(\Delta W/S \approx Kt)$ for longer periods at 1000 and 1100 °C. In this case, the large volume expansion that occurs during the reaction $TiB_2 \rightarrow TiO_2$ may cause cracking on the oxide layer, resulting in an increase in the active area for oxidation and in a heterogeneous diffusion in the barrier layer.

3.2.2. Al_2O_3–TiB_2 composite

The thermal stability of this material is directly related to the oxidation of the dispersoid particles, which are present on the surface and/or connected to the surface through open porosity channels. The weight gain curves (Fig. 3b) indicate diffusion-controlled kinetics, i.e. one-dimensional diffusion $(\Delta W/S)^2 \approx Kt$, at $T = 700$ and 800 °C, and two-dimensional diffusion $(1 - \alpha)\ln(1 - \alpha) + \alpha = Kt$ where $\alpha = \Delta W/S$, at $T \geqslant 900$ °C. Actually, the two-dimensional diffusion equation elaborated on the basis of a model for cylindrical particles, can justifiably be proposed to explain the phenomenologies in our system, as it shows the

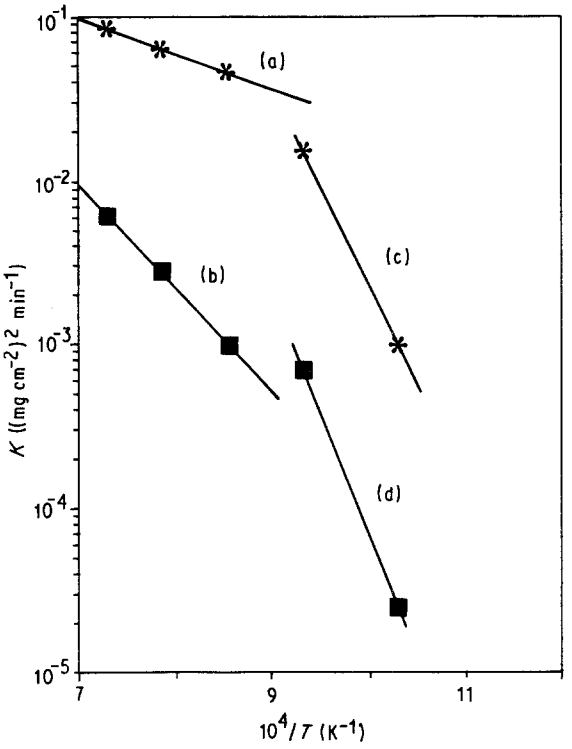

Figure 8 Arrhenius plots of the oxidation rate constants of (*) TiB_2 and (■) Al_2O_3–TiB_2. (a) 40 kJ mol^{-1}, (b) 125 kJ mol^{-1}, (c) 230 kJ mol^{-1}, (d) 330 kJ mol^{-1}.

development of needle-like particles starting from 700 °C, when the volume of the products is different from that of the reactants. Moreover, this second oxidation regime corresponds approximately to the temperature (≈ 900 °C) that allows the formation of a continuous oxide scale.

The Arrhenius plot of oxidation rate constants K versus temperature (Fig. 8) indicates a net change in the slope at $T \approx 900$ °C. For TiB_2, where diffusion-controlled mechanisms were found to be valid, the apparent activation energy is, at $T < 900$ °C, $E_a \approx 230$ kJ mol^{-1}, and at $T > 900$ °C, $E_a \approx 40$ kJ mol^{-1}. For Al_2O_3–TiB_2, at $T < 900$ °C (parabolic kinetics), $E_a \approx 330$ kJ mol^{-1}, and at $T > 900$ °C (two-dimensional-diffusion regime), $E_a \approx 125$ kJ mol^{-1}.

These values are in agreement with a change in the oxidation mechanism because they correspond to the overtaking of a more favourable reaction condition.

4. Conclusions

The oxidation of monolithic TiB_2 ceramic results in different behaviour and mechanisms depending on the temperature and time.

1. In the range $T \approx 400$–900 °C and in the first stage of the oxidation at 1000 and 1100 °C, the reaction is governed by a diffusion mechanism and crystalline TiO_2 and B_2O_3 are detected on the oxide scale.

2. During isothermal treatments at 1000 and 1100 °C, for longer than 8 and 13 h respectively, the increase of the active area for oxidation causes a mechanism governed by a linear law, the oxide scale being composed only of highly textured TiO_2 crystals.

With respect to the Al_2O_3–TiB_2 composite, weight gains for oxidation can be detected only at temperatures higher than 700 °C.

3. In the range from ~ 700–900 °C, a one-dimensional diffusion mechanism characterizes the rate-governing step of the oxidation reaction. TiO_2 (rutile) and $Al_4B_2O_9$ are the crystalline phases observed on the oxidized surfaces.

2. At $T > 900$ °C two-dimensional diffusion can be identified as the rate-governing step and the oxide scale is composed of highly oriented TiO_2 and $Al_{18}B_4O_{33}$.

References

1. S. BAIK and P. F. BECHER, *J. Amer. Ceram. Soc.* **70** (1987) 527.
2. V. J. TENNERY, C. B. FINCH, C. S. YUST and G. W. CLARK, in "Science of hard materials", edited by Viswanadham (Plenum, New York, 1983) pp. 891–909.
3. A. BELLOSI, T. GRAZIANI, S. GUICCIARDI and A. TAMPIERI, in "Proceedings of the 9th Special Ceramics Conference", London, December 1989 (Institute of Ceramics, UK) pp. 163–74.
4. J. MATSUSHITA, S. HAYASHI and H. SAITO, *J. Ceram. Soc. Jpn Inter. Ed.* **97** (1989) 1200.
5. I. KIMURA, N. HOTTA, Y. HIRAOKA and N. SAITO, *J. Eur. Ceram. Soc.* **5** (1989) 23.
6. A. BELLOSI and G. N. BABINI, in "4th International Symposium on Ceramic Materials and Components for Engines", Goeteborg, 10–12 June 1991, edited by R. Carlsson, T. Johansson and L. Kahlman (Elsevier Science, London).
7. J. MUKERJI and S. K. BISWAS, *J. Amer. Ceram. Soc.* **73** (1990) 142.
8. A. TAMPIERI, A. BELLOSI and V. BIASINI, in "Advanced Structural Inorganic Composites", edited by P. Vincenzini (Elsevier Science, Amsterdam, 1991) pp. 409–19.

Received 22 July 1991
and accepted 11 March 1992